

# A SUPERCONDUCTING MAGNETIC SHIELD FOR SRF MODULES WITH STRONG MAGNETIC FIELD SOURCES

J. Völker\*, A. Frahm, S. Keckert, J. Knobloch<sup>1</sup>, A.N. Matveenko, A. Neumann, H. Ploetz,  
Y. Tamashevich, Helmholtz Zentrum Berlin (HZB), Berlin, Germany  
<sup>1</sup>also at Universität Siegen, Siegen, Germany

## Abstract

Frequently SRF modules require strong focusing magnets close to SRF cavities. The shielding of those magnetic fields to avoid flux trapping, for example during a quench, is a challenge. At HZB, the bERLinPro photo-injector module includes a 1.4 cell SRF cavity placed in close proximity to a superconducting (SC) focusing solenoid. At full solenoid operation, parts of the double mu-metal shield are expected to saturate. To prevent saturation, we developed a new superconducting Meissner-Shield. Several tests of different designs were performed both in the injector module and in the HoBiCaT [1] test facility. The measured results of the final design show a significant shielding that are in good agreement with calculations. Based on these results, a reduction of the magnetic flux density in the mu-metal shields of almost one order of magnitude is expected. The design has now been incorporated in the injector module. In this paper we will present the design, the setup and results of the final testing of the superconducting shield.

## INTRODUCTION

A superconducting photoelectron injector [2] is currently under construction at HZB as electron source for SeaLab/bERLinpro. The main parts for the electron beam are the 1.4 cell SRF gun (incl. LHe tank and double Mu shield) and the superconducting (SC) solenoid for beam focusing. For best performance of space charge dominate electron beams the solenoid has to be positioned as close as possible to the SRF gun exit. Here the magnets fringe fields can interact with the outer Mu shield, consisting of Cryoperm [3]. In case of high flux densities, these high  $\mu_r$  metal plates can be saturated, which yields to a permanent magnetization and therefore a degradation of the shielding efficiency. In [3] these effects were studied and a first concept of an SC shield was introduced. It blocks most of the magnetic flux of the solenoid and prevent the Mu shields for saturation. Magnetic calculations predicted a shielding efficiency for the Mu shields of at least a factor of five.

## RESULTS OF THE FIRST DESIGN

The first SC shield design consists of a niobium plate, which should be installed as close as possible to the Mu Shield of the SRF gun. Furthermore the aperture for the beam tube should be as small as possible.

Figure 1 shows the setup of the ideal position between SRF gun flange and Mu shield. To meet these conditions the

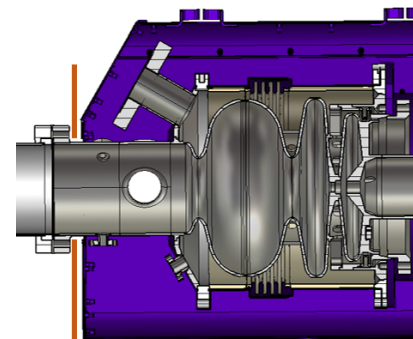


Figure 1: Drawing of the SC shield (brown) next to the Mu Shield (violet) of the SRF gun (grey).

shield has to be split into two identical pieces placed around the beam tube. The niobium plates are cooled down below the superconducting transition temperature  $T_C = 9.2$  K by two Cu plates, that are pressed together via an Aluminum frame work. The construction should passively cooled by connecting it with the gun flange ( $\approx 5$  K). However this concept was not sufficient. Therefore, an additional direct LHe cooling tube was installed in the aluminum framework. In a second cryogenic test the shield was cooled down below  $T_C$  and the magnetic fields produced by an SC solenoid next the SC shield were measured. Due to a heater connected to the LHe tubes the shield temperature could be briefly increased above  $T_C$ . The differences in the magnetic field for  $T_{\text{shield}} > T_C$  and  $T_{\text{shield}} < T_C$  were used to calculate the efficiency of the shield resulting in a value of  $\approx 1.3 \pm 0.3$ , which is far below of the expected value of roughly 5 of the magnetic calculations. The reason for this is the split design itself. To shield the magnetic field of the solenoid an azimuthal eddy current around the beam tube is necessary. However the mechanical contact between both niobium plates is not sufficient for the super currents between both plates. Due to the broken symmetry, the shielding efficiency is extremely decreased. These effects were studied as part of an improved model for the SC shield that used an electromagnetic solver like the low frequency (LF) solver of CST [4] instead of pure magnetic solvers. It was also used for the interpretation of the magnetic test of the new shield design and for studies of the shielding efficiency for the SRF gun Mu-shield.

## REDESIGN AND NEW INSTALLATION

To solve the issue of the broken azimuthal symmetry the shield needs a single niobium plate. One feature hereby is the

\* jens.voelker@helmholtz-berlin.de

increased aperture diameter of at least the outer gun flange diameter (80mm). The other components of the shield, like the cooling frame work, cooling tubes and the Cu plates were reused. The final construction can be seen in Fig. 2.

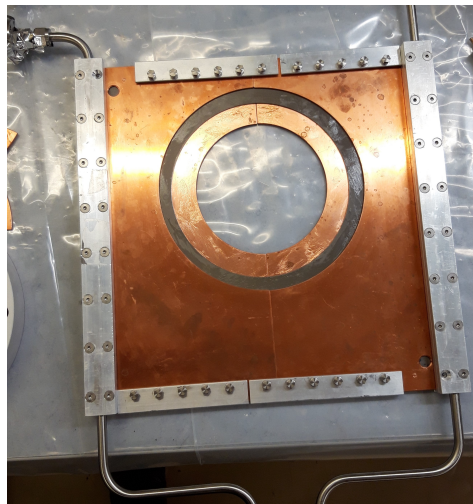


Figure 2: Image of the shield construction with the Niobium plate between both Cu cooling plates and connected to the cooling tubes.

This new shield design was installed in the HoBiCaT cryostat together with the SC solenoid 1.0<sup>1</sup>. For an easier installation of all sensors and connections the whole setup was installed horizontally, with the solenoid on top of the shield in a distance of 65mm - similar to the later setup in the SRF injector. An image of the mechanical construction can be seen in Fig. 3.

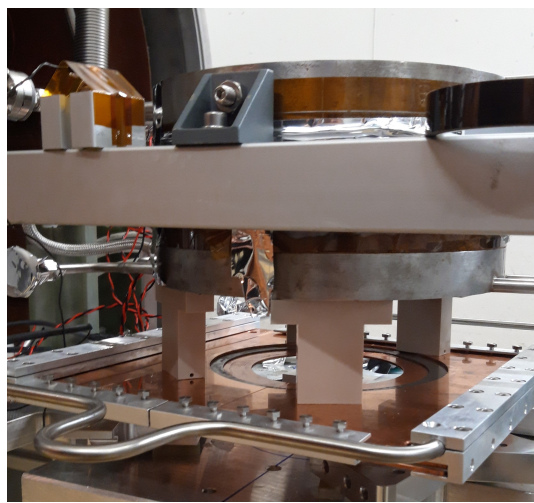


Figure 3: Image of the horizontal test setup inside the HoBiCaT cryostat (side view). SC solenoid magnet on top of the SC shield held by an aluminum frame work and aligned to the SC shield by three 65mm plastic spacer.

<sup>1</sup> This solenoid has a max. operation current of 7 A. For the Gun Module, the solenoid 1.1 will be used, which has a similar field distribution but less coil windings. Solenoid 1.1 has a max. operation current of 20 A.

Due to the limitation of the 4.2 K LHe systems in HoBiCaT, Solenoid and shield must be connected in series to a single LHe line. A heater at the LHe line downstream of the solenoid was used to increase the temperature of the shield above  $T_C$ . For the measurement of the magnetic field distribution, three flux gate sensors below the SC shield, four Hall sensors chips around the plate and four CERNOX sensors (three on the surface of the Niobium plate and one at the solenoid yoke) were installed, which is illustrated in Fig. 4. The flux gate sensors can be measure extreme small field variation of less than 1  $\mu$ T, but have an upper operation limited of 500  $\mu$ T and can be used in cryogenic and room temperature (RT).

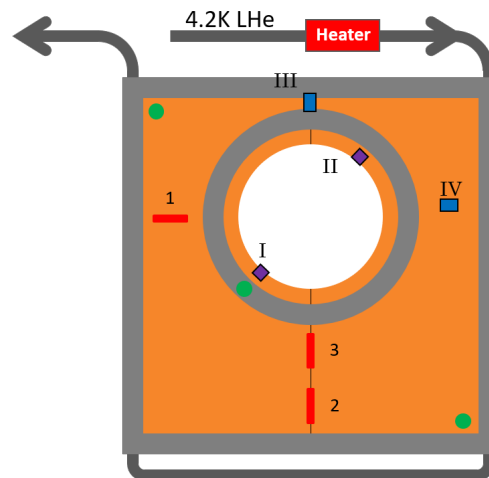


Figure 4: Setup of the SC shield in HoBiCaT (top view - Solenoid above). Inclusively, cooling tubes for 4.2 K LHe cooling and the heater to warm up the shield above  $T_C$ . (green) CERNOX temperature sensors, (red) 1D Bartington Flux Gate Sensors [5]- below shield, (violet) 1D Hall Sensors I and II perpendicular to the shield, (blue) 1D Hall sensors parallel to the shield.

The hall sensors chips consist of SMD Hall sensors and a PT100 sensor on a small PCB. The hall sensors have a resolution of only 100  $\mu$ T but can be operated up to 2 T with a good linear correlation between flux density and voltage signal over the whole range. However the correlation coefficient (Hall parameter) and the signal offsets are not well defined for cryogenic temperatures, but they are constant during a stable thermal operation. All magnetic sensors, as well as the solenoid parameters were read out by a multichannel ADC (IMC system [6]) with a frequency of 200 Hz.

## MEASUREMENTS AND DATA ANALYSIS

After installation of the test setup in HoBiCaT two measurement runs were performed. During each run different thermal and magnetic conditions were tested. The temperature of the SC shield could be varied between 5 K and 25 K. In case of a quite stable temperature the solenoid current was ramped several times. Figure 5 shows an example of one of these runs with three general setups:

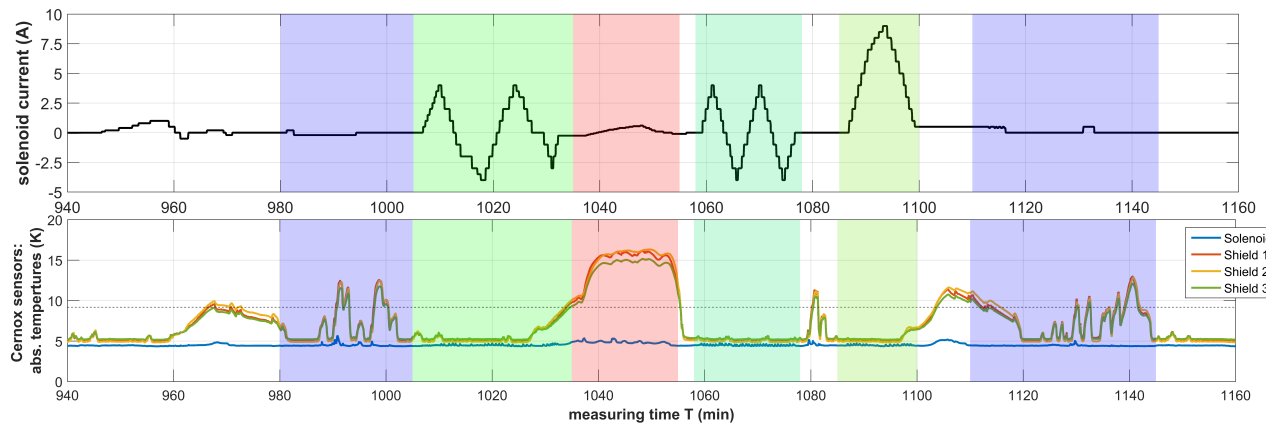


Figure 5: Overview of the first test run of the SC-shield Test in HoBiCaT. (top) measured solenoid current at the power supply. (below) measured temperatures of the shield and the solenoid. The four different test scenarios are highlighted by color code (see text).

- Solenoid cycle with  $T_{\text{shield}} < T_C$  (green marked)
- Solenoid high current test with  $T_{\text{shield}} < T_C$  (light green marked)
- Solenoid cycle with  $T_{\text{shield}} > T_C$  (red marked)
- constant Solenoid current and  $T_{\text{shield}}$  passing  $T_C$  (blue marked)

The first test setup can be subdivided into scenarios with none or different solenoid currents during the phase transition of the shield ( $T_{\text{shield}} > T_C \Rightarrow T_{\text{shield}} < T_C$ ).

As a first step of the data analysis, the temporal sensor signals must be corrected for undesired eddy currents in the setup. They result from the massive Cu cooling bobbin of the SC solenoid and are visible as a delay (exponential decay) between the signals of the magnetic sensors and the solenoid current after a current change. This issue is driven by the small ohmic resistance of the bobbin at LHe temperature, the large inductivity of the solenoid itself and the strong magnetic coupling between coil and bobbin. It can be mathematically described by a transformer equation, resulting in a value of  $\approx 180\text{ms}$  for the given values of the used solenoid. The sum of the measured coil current and the induced bobbin current can be calculated by this transformer model. Only this effective magnet current is directly correlated to the magnetic field of the solenoid and therefore with the sensor data. Figure 6 shows two examples for one flux gate and Hall sensor data after this eddy current correction.

All sensor data are well linear correlated and show significant differences for both shield temperatures. Firstly, the magnetic polarity of the field below the shield changes if the Niobium transit into the superconducting state. Also the absolute slope values are significantly decreased. All sensor signals as function of the effective solenoid current were linear fitted for each sensor and each setup individually. The resulting linear slope for one sensor depends only on the current state of the shield (NC or SC) and the position of the sensor itself. Only in the high current test, a slight non-linearity was visible for currents above the maximum possi-

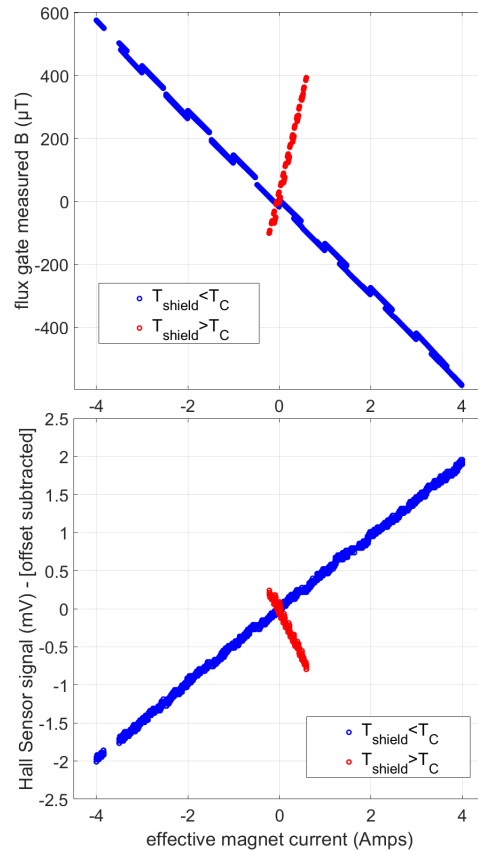


Figure 6: Example of a fluxgate (top) and Hall sensor (bottom) data as function of the calculated effective magnet current. For each sensor the measured data is plotted for shield temperatures below and above  $T_C$  of Niobium.

ble operating current in the gun module. Table 1 shows the mean values of the fit results for each sensor. Here it can be seen that the relative change of the absolute slope values is in a range between a factor of 2 and roughly 10. Experimental settings where the solenoid magnet is running during the

NC-to-SC transit of the shield (Meissner-Ochsenfeld-effect) produce only an additional offset in the sensor data, but did not change these slope values.

Table 1: Average Slope Values of all Linear Fits for the Sensor Signal

Sensor	$T_{\text{shield}} < T_C$	$T_{\text{shield}} > T_C$	unit
FG 1	$-142.2 \pm 1.7$	$+645.6 \pm 3.1$	
FG 2	$+41.1 \pm 0.6$	$-351.9 \pm 1.9$	$\frac{\mu\text{T}}{\text{A}}$
FG 3	$+103.0 \pm 0.8$	$-775.6 \pm 0.1$	
Hall I	$+0.480 \pm 0.007$	$-1.255 \pm 0.015$	
Hall II	$-1.163 \pm 0.004$	$+0.875 \pm 0.005$	$\frac{\text{mV}}{\text{A}}$
Hall III	$-0.338 \pm 0.008$	$+0.640 \pm 0.010$	
Hall IV	$-0.033 \pm 0.004$	$+0.385 \pm 0.005$	

These results cannot be used for a general interpretation of the achievable shield efficiency, because of the extreme variations of the slope as a function of the sensor position and the missing magnetic interaction with a  $\mu_r$  material. Therefore a CST model was implemented to interpret the measured ratios.

## CST MODEL AND RESULTS

Main components for this model are also here the Niobium plate and the solenoid magnet. Instead of the magnetic solver, the LF solver of CST was used to include the effects of eddy currents. The Niobium plate was defined with a variable conductivity  $\sigma$  between  $\sigma_{\min} \approx 0(\Omega\text{m})^{-1}$  (insulator) and  $\sigma_{\max} = 1e16(\Omega\text{m})^{-1}$  (superconductor). Also, the materials of the solenoid magnet were implemented with special condition to neglect all eddy currents but in the shield. Therefore, yoke and Cu bobbin were defined with nearly zero conductivity values so that only the magnetic behavior of the iron yoke was used for the field calculations. The used frequency range for the LF solver is based on the current ramps during the real solenoid operation ( $\approx 0.5 \text{ A/s}$ ) which results for 0.5 A step (quarter wave) to  $\approx 0.25 \text{ Hz}$ . A scan of the shield conductivity  $\sigma$  were performed for each frequency to ensure that the solutions for  $\sigma_{\min}$  and  $\sigma_{\max}$  are stable and not part of the transition region.

This model was expanded by further components according to the experimental setup. For the HoBiCaT test, a finer vacuum mesh grid was implemented around the shield plate and next to the measured sensor positions, to compare the shield model with the experimental results. In case of the later module installation, the front part of the Gun-Mu-shield and a short SC beam tube was implemented as it can be seen in Fig. 7. The Mu shield material was also defined without any conductivity only with high  $\mu_r$  values of  $\approx 20000$ . With this model also geometrical parameters can be variated like the inner aperture or the outer dimensions of the shield (e.g. local quench of the shield edges)

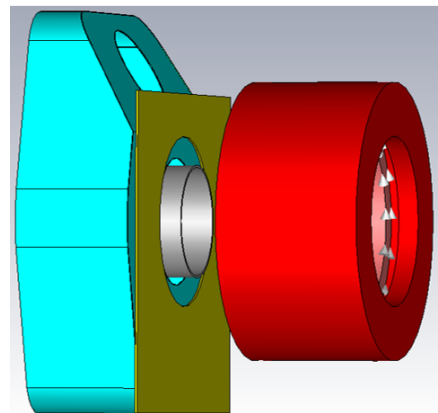


Figure 7: Design of the advanced CST model inclusively the Mu shield front (blue), the SC dummy tube (gray), SC shield (green) and solenoid (red).

## Analysis Shield Test

Due to the different sources of sensor offsets in the experimental data, a direct reconstruction of the measurements with CST calculations is not effective. Instead we tried to reconstruct the relative field behavior, like the correlated field changes with a solenoid scan or the ratio between superconducting and normal-conducting shield measurement.

Therefore we used the fitted sensor data slopes  $B'_{\text{ref}}$  from Table 1 and try to find consistent values  $B'_{\text{mod}}$  in the CST model next to the measured positions in the experimental setup (reference position  $P_{\text{ref}}$ , model coordinates  $P_{\text{mod}}$ ).

- find all mesh coordinates  $P_{\text{mod}}$ , where  $|B'_{\text{ref}} - B'_{\text{mod}}| < \Delta$  the expected uncertainty.
- calculates the distances  $d = |P_{\text{ref}} - P_{\text{mod}}|$  to all these model coordinates
- calculate the average distance  $D$  to the nearest six neighbors

One example of such an analysis for the flux gate sensor 1 can be seen in Fig. 8. Here, the minimum distance is plotted as color code as function of the necessary uncertainty  $\Delta$  and the aperture radius of the SC shield. It shows that the measurement results of this sensor can be found in the CST model quite next to the reference coordinate with very small uncertainties in the permille range. Especially for aperture radii between 80 and 86 mm model and measurement matches very good (SC shield aperture is 80 mm). For almost all 7 sensors this plot looks similar. Only Hall sensor 4 shows extreme differences or huge necessary uncertainties. However, this sensor measured extreme small magnetic flux densities when the shield temperature is below  $T_C$ , producing extreme measurement uncertainties. Nevertheless this result shows that the CST model is in good agreement to the measurements of the shield test in HoBiCaT. As a last step this confirmed model was used to study the shielding efficiency of the flux reduction in the gun Mu-shield.

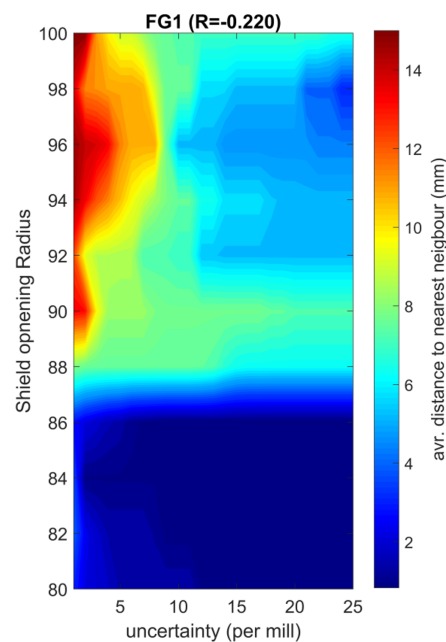


Figure 8: Example of analysis between the fitted experimental values and CST calculations for the flux gate sensor 1.

### Calculated Shielding Efficiency

Here we used the advanced model as it is illustrated in Fig. 7. First calculations with  $\sigma \approx 0$  show that the most intensive interaction between solenoid field and the Mu shield take place in the two front planes of the Mu shield. The magnetic flux density in these regions can achieve values of more than 1T for solenoid currents in the range of specified operation range. Here you have to keep in mind that the saturation level of the used Cryoperm is in the range of 0.87T. Different parameter combination of the model were studied, but the most relevant combinations are when SC shield and dummy tube are both superconducting or normal conducting. The comparison of both results are shown in Fig. 9. Here the absolute flux density in the Mu shield material is plotted with the same color code in case of NC (left) and SC (right). The region with the highest values is next to the chimney opening for the LHe tank. Especially in this region the magnetic flux will be significantly reduced by more than one order of magnitude. Due to the SC shield the maximum flux density in the Mu shield plates can be decreased to  $\approx 140$  mT which is far below the saturation value.

### CONCLUSION

An SC shield was developed blocking the magnetic fringe fields of the SC solenoid and prevent the Mu shields for saturation. Two shield designs were tested under real conditions using the SC gun solenoid in the Gun module itself and in HoBiCaT. Several magnetic sensors measured the magnetic flux density next to the shield. Unwanted effects of eddy

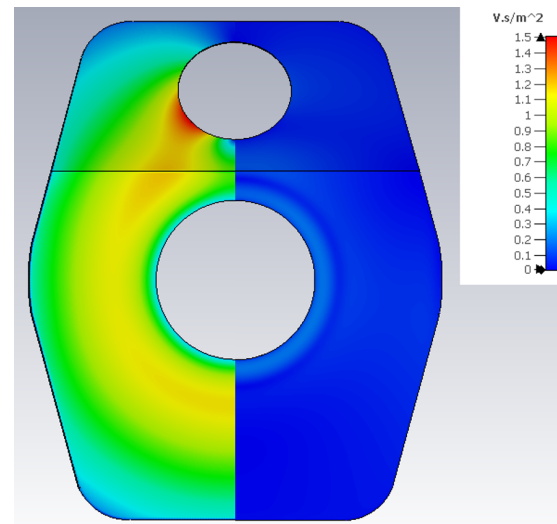


Figure 9: Combined image of two CST solutions for the model shown in Fig. 7. The color code shows the calculated magnetic flux density inside the Cavity Mu-shield in case of the Niobium plate is normal conducting (left) and superconducting (right).

currents inside the solenoid were reduced from the sensor signals by a transformer analysis. All sensor signals are well linear correlated to the magnet current up to the maximum operating current (no hard quench). A CST model of the test setup was implemented, used as reference for the interpretation of the measurements. Both are in good agreement to each other. Further calculation with the advanced model including the Mu shield of the gun, show a shielding efficiency of roughly a factor of 10 in regions with extreme high flux densities. In the next months the SRF gun module will be assembled after gun repair [7] and the new SC shield will be a new and important component of the cold string.

### REFERENCES

- [1] O. Kugeler, W. Anders, J. Knobloch, and A. Neumann, "CW adaptation of TESLA technology in HoBiCaT," in *Proc. IPAC'10*, Kyoto, Japan, 2010. doi:10.18429/JACoW-IPAC2010-WEPEC004
- [2] A. Neumann *et al.*, "Towards a 100mA superconducting RF photoinjector for bERLinPro," in *Proc. SRF'13*, Paris, France, 2013. doi:10.18429/JACoW-SRF2013-M01OB02
- [3] J. Voelker *et al.*, "A superconducting magnetic shield for the photoelectron injector of BERLin-Pro," in *Proc. SRF'19*, Dresden, Germany, 2019. doi:10.18429/JACoW-SRF2019-MOP105
- [4] CST Studio Suite, <https://www.3ds.com>
- [5] Flux gate sensors, Bartington-01H, <https://www.bartington.com/mag-01h>
- [6] IMC Meßsysteme GmbH, Berlin, <https://www.imc-tm.de>
- [7] Y. Tamashevich, "Damage recovery for SRF photoinjector cavities," presented at the *20th Int. Conf. on RF Superconductivity (SRF'21)*, Grand Rapids, MI, USA, virtual conference, Jun. 2021, paper WEOCAV07, this conference.